39. B. Fauqué *et al.*, *Phys. Rev. Lett.* **96**, 197001 (2006).
40. J. Xia *et al.*, *Phys. Rev. Lett.* **100**, 127002 (2008).

Acknowledgments: This work was performed partly at the Advanced Resonant Spectroscopies (ADRESS) beamline of the Swiss Light Source, using the Super Advanced X-ray Emission Spectrometer (SAXES) instrument jointly built by Paul Scherrer Institut (Villigen, Switzerland), Politecnico di Milano (Italy), and École Polytechnique Fédérale de Lausanne (Switzerland); partly at the ID08 beam line of the ESRF (Grenoble, France); partly at the UE46-PGM1 beamline of Bessy-II (Helmholtz-Zentrum Berlin für Materialien und Energie, Germany); and partly at the Resonant Elastic and Inelastic X-ray Scattering (REIXS) beamine at the Canadian Light Source (CLS; Saskatoon, Saskatchewan, Canada). Part of this research project has been supported by the European Commission under the 7th Framework Programme: Research Infrastructures (grant agreement number 226716), the European project "SOPRANO" under Marie Curie actions (grant no. PITNGA-2008-214040), the German Science Foundation under SFB/TRR 80, and by the Italian Ministry of Research [Ministero dell'Istruzione, Università e Ricerca (MIUR), grant no. PRIN-20094W2LAY]. The research at the CLS is supported by the Natural Sciences and Engineering Research Council of Canada, the National Research Council, the Canadian Institutes of Health Research, and the Univ. of Saskatchewan. We gratefully thank S. Kivelson, T. Devereaux, S. Sebastian, M.-H. Julien, and G. Khaliullin for discussions; T. Schmitt, K. Zhou, and C. Monney for support at the ADRESS beamline; and V. Hinkov, C. Lin, M. Bakr, M. Raichle, and D. Haug for preparation of some of the single-crystal samples. M.S. acknowledges additional funding from the CNR Institute and from the European Union Community.

Supplementary Materials
www.sciencemag.org/cgi/content/full/science.1223532/DC1
Materials and Methods
Figs. S1 to S4
Table S1
References (*41*–*51*)

18 April 2012; accepted 2 July 2012
Published online 12 July 2012;
10.1126/science.1223532

Long-Range Ordered Carbon Clusters: A Crystalline Material with Amorphous Building Blocks

Lin Wang,[1,2]* Bingbing Liu,[2] Hui Li,[3] Wenge Yang,[1] Yang Ding,[4] Stanislav V. Sinogeikin,[5] Yue Meng,[5] Zhenxian Liu,[6] Xiao Cheng Zeng,[3] Wendy L. Mao[7,8]

Solid-state materials can be categorized by their structures into crystalline (having periodic translation symmetry), amorphous (no periodic and orientational symmetry), and quasi-crystalline (having orientational but not periodic translation symmetry) phases. Hybridization of crystalline and amorphous structures at the atomic level has not been experimentally observed. We report the discovery of a long-range ordered material constructed from units of amorphous carbon clusters that was synthesized by compressing solvated fullerenes. Using x-ray diffraction, Raman spectroscopy, and quantum molecular dynamics simulation, we observed that, although carbon-60 cages were crushed and became amorphous, the solvent molecules remained intact, playing a crucial role in maintaining the long-range periodicity. Once formed, the high-pressure phase is quenchable back to ambient conditions and is ultra-incompressible, with the ability to indent diamond.

Carbon materials—such as graphene, graphite, diamond, fullerenes, and carbon nanotubes, as well as nanostructured and amorphous carbon—display a remarkable range of mechanical, electronic, and electrochemical properties that have led to many advanced applications (*1*–*7*). The structures of all of these materials are either ordered (crystalline) or disordered (amorphous). Polymeric fullerenes have been synthesized at different pressures and temperatures when pure C_{60} or C_{70} were used as starting materials (*8*–*11*). Under cold (ambient temperature) compression, the C_{60} cages collapse, and the crystalline C_{60} phase transforms into amorphous carbon above 30 GPa (*12*, *13*). Under high-temperature compression, pure C_{60} forms different polymerized structures, with the C_{60} cages transforming into graphitic carbon or a mixture of sp^2 and sp^3 amorphous phases. Some of these phases are also ultrahard (*8*, *11*, *14*, *15*).

Another type of starting material, solvated C_{60}, which is composed of C_{60} molecules separated by solvent molecules, has received considerable attention (*16*–*18*). The solvated fullerenes are crystalline materials with high stability, tunable metrics, and functionality. The incorporation of guest molecules into the host C_{60} lattice changes the crystal structure. The changes are also reflected in their vibrational properties and, consequently, the Raman and IR (infrared absorption) spectra (*19*). It was reported that the guest molecules can hinder the rotation of the C_{60} molecules, leading to a decrease in their vibrational-rotational couplings (*20*, *21*). Furthermore, the interactions between C_{60} and the guest molecules reduce the icosahedral symmetry of the C_{60} molecules, allowing electronic transitions that are forbidden in pristine C_{60} and inducing a strong photoluminescent response (*22*).

C_{60}**m*-xylene, an important solvated C_{60} with greatly enhanced photon luminescence (*18*, *22*), was selected for this investigation. It was studied up to 60 GPa by using a diamond anvil cell. X-ray diffraction (XRD), Raman spectroscopy, infrared absorption spectroscopy, and inelastic x-ray scattering (IXS, also called x-ray Raman spectroscopy) were used to analyze the crystal structure, lattice vibration, and bonding type of the material at high pressures. Independent quantum molecular dynamics (QMD) simulations were also carried out to understand and provide insight into the phase transformation of the material under high pressure.

We used XRD to reveal long-range structural order. Detailed information about the experiments is shown in the supplementary materials. Typical XRD patterns of the C_{60}**m*-xylene during compression are shown in Fig. 1. The XRD pattern at ambient pressure is well indexed as individual C_{60} molecules occupying the lattice points of a hexagonal close-packed (hcp) structure (space group $P6_3$) with lattice constants a = 2.3761 nm and c = 1.0120 nm, in good agreement with literature values (*18*, *22*, *23*). During compression up to 60.1 GPa, the diffraction peaks gradually broaden, weaken, and shift to higher Q (reciprocal lattice vector). No drastic change was observed, indicating that the hcp periodicity of the molecules

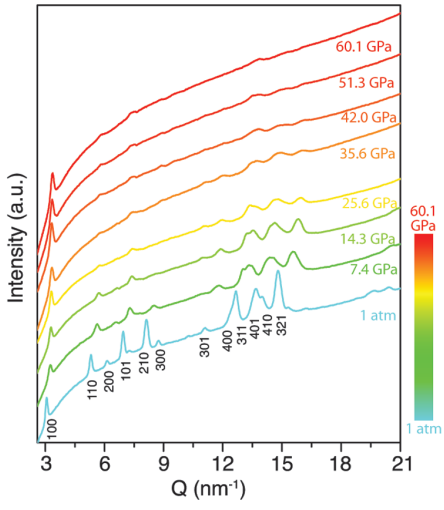

Fig. 1. XRD patterns of C_{60}**m*-xylene at different pressures. The numbers below the 1-atm XRD pattern indicate the indexing for the hcp structure. The pressures for the XRD patterns are given by the colored numbers at the right and in the bar.

[1]High Pressure Synergetic Consortium (HPSynC), Geophysical Laboratory, Carnegie Institution of Washington, Argonne, IL 60439, USA. [2]State Key Laboratory of Superhard Materials, Jilin University, Changchun 130012, China. [3]Department of Chemistry, University of Nebraska, Lincoln, NE 68588, USA. [4]Advanced Photon Source, Argonne National Laboratory, Argonne, IL 60439, USA. [5]High Pressure Collaborative Access Team (HPCAT), Geophysical Laboratory, Carnegie Institution of Washington, Argonne, IL 60439, USA. [6]Geophysical Laboratory, Carnegie Institution of Washington, Washington, DC 20015, USA. [7]Geological and Environmental Sciences, Stanford University, Stanford, CA 94305, USA. [8]Photon Science and Stanford Institute for Materials and Energy Sciences, SLAC National Accelerator Laboratory, Menlo Park, CA 94025, USA.

*To whom correspondence should be addressed. E-mail: lwang@ciw.edu

remains intact. This is in contrast to pure C_{60}, where the face-centered cubic periodicity of the C_{60} molecular units disappears when it amorphizes above 30 GPa (*13*).

We employed Raman spectroscopy to study the local structure of ordered amorphous carbon clusters (OACC) recovered from high pressures. The Raman spectrum of pristine C_{60}**m*-xylene has 10 Raman-active modes ($2A_g$ and $8H_g$), as labeled in the Fig. 2A, arising from the intramolecular vibrations of C_{60} and some other weak peaks located from 300 to 550 cm^{-1}, which originate from the van der Waals interactions between C_{60} and the *m*-xylene molecules. Figure 2A shows the Raman spectra of the pristine sample and the samples decompressed from different pressures. As shown in the spectrum at 13 GPa, all of the vibrational bands that correspond to the caged structure remained, suggesting the preservation of the C_{60} cages. No peak shift was observed for the $A_g(2)$ mode, indicating that no pressure-induced polymerization occurred in the solvated C_{60} because the C_{60} cages are isolated from each other by the solvents (*11*). However, in the spectrum of the sample decompressed from 32 GPa, only a few strong bands from the C_{60} were observed, and all of the other bands disappeared. At the same time, a new band originating from the amorphous carbon appeared and became dominant at higher pressures. These observations suggest that C_{60} cages start to collapse at 32 GPa and completely transform into amorphous carbon clusters at higher pressures (*12*, *13*).

The two broad bands preserved in the spectrum of the sample decompressed from 32 GPa contain three Raman peaks correspond to the pentagon shear [$H_g(7)$], pentagon pinch [$A_g(2)$], and hexagon shear [$H_g(8)$] modes, respectively (*8*, *9*, *11*). The vibrational modes related to the breathing modes (at lower wave numbers) of the cage disappear. These changes suggest that C_{60} cages start to break into fragments and lose the cage symmetry, but the pentagon and hexagon rings are still preserved in the fragments, as evidenced from the Raman peaks observed in the recovered sample. At higher compression, the fragments are increasingly broken up, and thus we only observe a very broad peak from amorphous carbon.

We further studied the bonding change of the sample during the phase transformation by using IXS. The experimental details and spectra (fig. S1) are included in the supplementary materials. As labeled in the figure, both π* and σ* peaks, which correspond to sp^2 and sp^3 bonds, were observed in the spectra at relatively low pressures, and no obvious change in peak intensities was observed below 26 GPa (*6*). At higher pressures above 36 GPa, the π* peak became too weak to be observed, suggesting the complete bonding transition from sp^2 to sp^3 caused by the collapse of C_{60} cages as observed by the Raman spectroscopy. The IXS spectrum of OACC recovered from 42 GPa shows a π* peak that is much weaker in intensity compared with lower compressions, suggesting that a portion of sp^3 bonding transforms back to sp^2 upon decompression while the rest is preserved to the ambient pressure. This implies that OACC has mixed bonding with both sp^2 and sp^3.

The ability to preserve the high-pressure structure back to ambient conditions is important for future practical applications. Figure 2B shows XRD patterns of a pristine sample and the samples decompressed from different pressures. We found that at pressures below ~30 GPa, the C_{60} cages survive and are recovered upon decompression. As the applied pressure is increased, the C_{60} cages start to be irreversibly crushed, and this disorder is preserved back at ambient pressure. The C_{60} cages completely collapse and transform into amorphous clusters at pressures above 32 GPa, but the overall hcp lattice is preserved, forming OACC (Fig. 2C). The XRD for the decompressed OACC retains long-range periodicity similar to the pristine material. As shown in the figure, OACC recovered from 35 GPa has a hcp structure (space group $P6_3$) with $a = 2.404$ nm and $c = 1.014$ nm. The lattice is slightly larger than the pristine structure due to the collapse of the C_{60} cages. In addition, there are several broad bands (indicated by the dashed lines) that coexist with the sharp diffraction peaks in the spectra of the decompressed samples. Because the background has been carefully subtracted during the measurements, the broad bands represent the contribution from the amorphous carbon clusters, which is consistent with the local disorder observed in the Raman studies. The center position of the first band is ~4.4 Å, which is different from glassy carbon and other amorphous carbons that possess some short-range order. Although the physical meaning of the first sharp peak of an XRD pattern from an amorphous material is not completely understood, the difference still suggests that the amorphous carbon clusters in OACC have different local structure with glassy carbon and other amorphous carbons due to their extremely small size and different local environments.

Previous experimental and simulation results suggest that the solvent molecules are placed along the three-fold axis of the lattice (*22*, *23*). Therefore, the C_{60} cages are isolated from each other by the solvent. Although the C_{60} cages collapse at high pressures, the carbon clusters likely stay on the lattice sites and maintain the periodic structure due to the presence of the solvent molecules (fig. S2). This finding suggests that the solvent plays a crucial role in maintaining the long-range periodicity in OACC. The solvent in the solvated fullerenes can be easily removed by a heat treatment (*18*). Figure S3 in the supplementary materials shows the XRD pattern of the decompressed material after a mild heat treatment

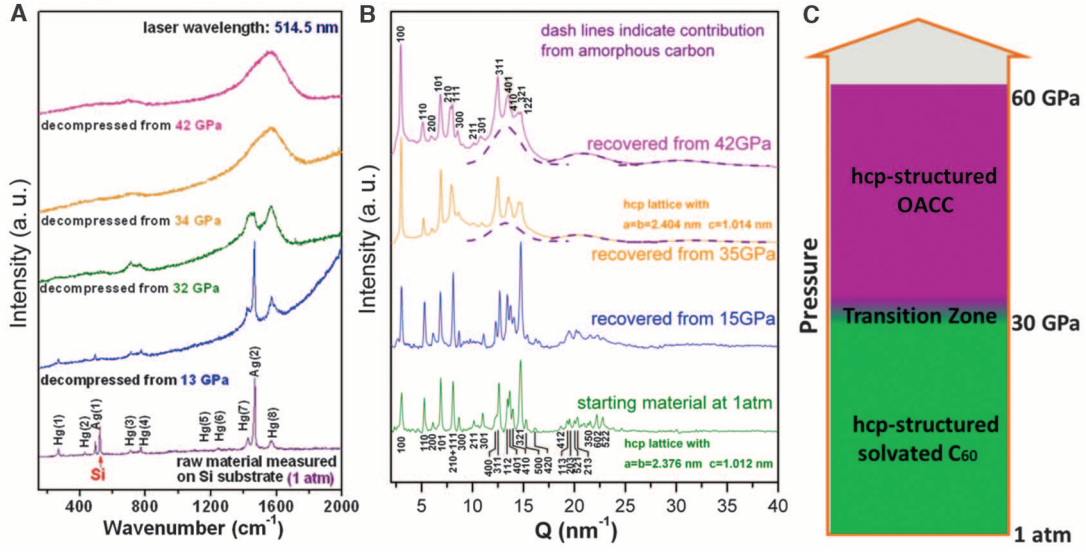

Fig. 2. Raman spectra and XRD patterns of samples decompressed from different maximum pressures and the phase diagram at room temperature. (**A**) The Raman spectra were gathered using a 514.5-nm excitation laser line. In the spectra of the samples quenched from pressures above 32 GPa, all the bands belonging to C_{60} disappeared and a new band originating from the amorphous carbon appeared and became dominant. (**B**) The backgrounds were carefully subtracted during the measurement of the XRD patterns. There are several broad bands (indicated by the dashed lines) that represent the contributions from the amorphous carbon clusters and coexist with the sharp diffraction peaks from the hcp lattice. (**C**) The phase diagram shows that below about 30 GPa the C_{60} cages survive and can be recovered upon decompression. At higher pressures, the C_{60} cages start to irreversibly break and transform into hcp-structured OACC.

at 107°C for 8 hours. The material loses its long-range periodicity and transforms into an amorphous structure after the solvent is evaporated, further confirming the critical role of the solvent in maintaining long-range periodicity. Furthermore, the structure of solvated fullerenes (e.g., C_{60} and C_{70}) is solvent dependent. An extensive class of crystalline-solvated fullerenes can be obtained by changing the solvent species and the ratio of fullerenes to solvent (*22*). This result suggests that one may be able to synthesize a series of carbon materials with this unique structure, but with different packing symmetry and carbon cluster size, by selecting different fullerene cages.

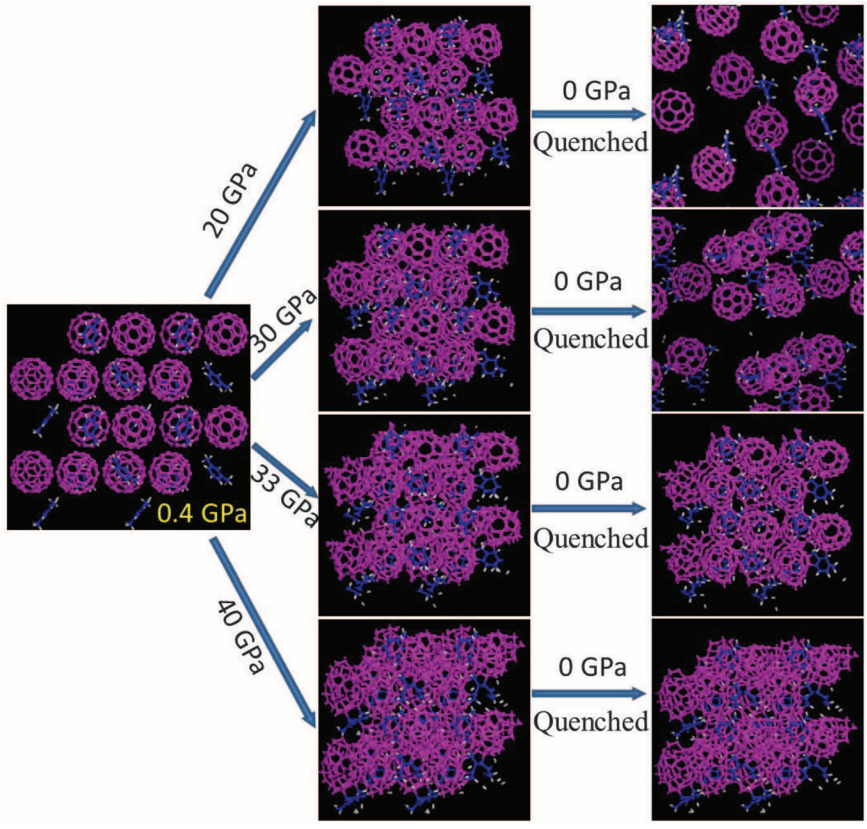

Fig. 3. Simulated structures of the material under different compression and decompression conditions. Far left, the pristine structure at 0.4 GPa. The deformation of the C_{60} cages is elastic below ~30 GPa, and the deformed cages return to their initial shape as they are decompressed back to ambient pressure. Above 30 GPa, many carbon-carbon bonds start to break, and the cages can no longer return to C_{60} upon decompression. OACC maintains long-range periodicity and can be preserved under ambient pressure conditions.

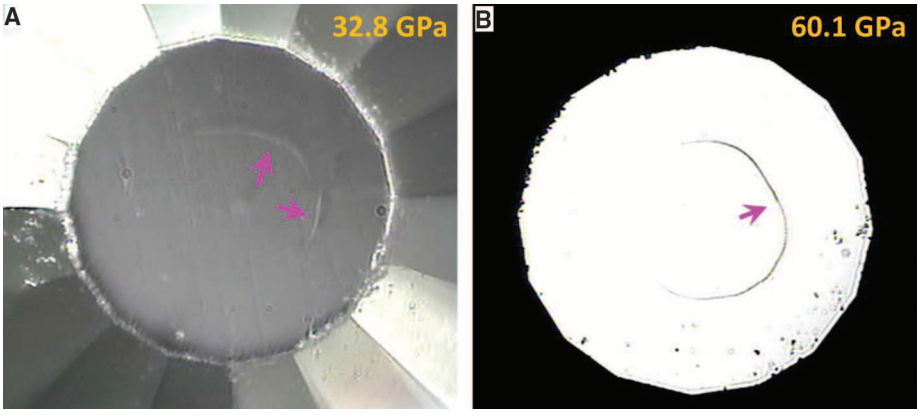

Fig. 4. Optical photomicrographs of the ring cracks in the diamond anvils generated after formation of OACC and then release of the pressure. The diamonds were carefully cleaned using sandpaper. The maximum pressures were 32.8 (**A**) and 60.1 GPa (**B**). As marked by the arrows, the ring cracks follow the original boundary of the samples in the gaskets.

The experiments show the phase transformation and evidence for the existence of OACC. To demonstrate that the experimentally observed OACC is a generic phenomenon, and to provide molecular-level insight into how this new material forms at high pressure, we performed independent QMD simulations using a similar close-packing (face-centered cubic) system as a test model system. Detailed information about the calculation is shown in the supplementary materials. Figure 3 shows the structures of the materials at different pressures and upon decompression. Below ~30 GPa, the deformation is elastic. The deformed cages return to their initial shapes as they are decompressed back to ambient pressure. However, above 30 GPa, the deformation becomes so large that a phase transition is triggered, and C_{60} molecules start to collapse by breaking the sp^2 hybrid C-C double bonds and forming new sp^3 hybrid C-C bonds. The spherical-shaped C_{60} molecules are also changed to the ellipsoidal structure. As a result, the cages can no longer return to their initial structure upon decompression. At even higher pressures (>35 GPa), the C_{60} cages completely collapse and transform into highly disordered carbon clusters forming OACC; OACC maintains the long-range periodicity due to the presence of the solvent molecules and can be preserved back to ambient pressure conditions. The pressure-induced phase transition seen in QMD simulations at about 32 to 33 GPa is consistent with that observed in the experiments, thereby offering additional insight into the local structure of the new material, as well as physical and chemical mechanisms of this phase transition.

Finally, it is important to note that OACC created ring crack indentations on the diamond anvils. These indentations follow the original boundary of the sample in the gasket, indicating the exceptional hardness of the new phase (*4*, *5*). Two optical pictures of the ring cracks generated after releasing from pressures of 32.8 and 60.1 GPa are shown in Fig. 4. From previous studies, ring cracks have only been observed when a diamond anvil is indented by another superhard material, such as an opposing beveled diamond anvil. The observation of ring cracks indicates that OACC has ultra-incompressibility comparable to diamond. The shift of the strongest XRD peak of the high-pressure phase as a function of pressure was also analyzed (fig. S11). Comparison with diamond also suggests that OACC is as incompressible as diamond.

In conclusion, we synthesized a carbon material, from units of amorphous carbon clusters and solvent molecules organized on a crystalline lattice, with the incompressibility comparable to diamond. OACC has long-range periodicity but is locally disordered, with the solvent molecules playing a crucial role in maintaining the long-range periodicity. It can also be preserved back to ambient conditions. Simulations provide additional insight into the formation mechanism that are consistent with the experimental results.

References and Notes

1. H. W. Kroto, J. R. Heath, S. C. O'Brien, R. F. Curl, R. E. Smalley, *Nature* **318**, 162 (1985).
2. S. Iijima, *Nature* **354**, 56 (1991).
3. K. S. Novoselov *et al.*, *Science* **306**, 666 (2004).
4. W. L. Mao *et al.*, *Science* **302**, 425 (2003).
5. Z. W. Wang *et al.*, *Proc. Natl. Acad. Sci. U.S.A.* **101**, 13699 (2004).
6. E. D. Miller, D. C. Nesting, J. V. Badding, *Chem. Mater.* **9**, 18 (1997).
7. M. Wu, X. J. Wu, Y. Pei, Y. Wang, X. C. Zeng, *Chem. Commun.* **47**, 4406 (2011).
8. Y. Iwasa *et al.*, *Science* **264**, 1570 (1994).
9. C. S. Yoo, W. J. Nellis, *Science* **254**, 1489 (1991).
10. M. N. Regueiro, P. Monceau, A. Rassat, P. Bernier, A. Zahab, *Nature* **354**, 289 (1991).
11. B. Sundqvist, *Adv. Phys.* **48**, 1 (1999).
12. F. Moshary *et al.*; de Vries MS, *Phys. Rev. Lett.* **69**, 466 (1992).
13. L. Wang *et al.*, *Appl. Phys. Lett.* **91**, 103112 (2007).
14. L. Marques *et al.*, *Science* **283**, 1720 (1999).
15. M. Núñez-Regueiro, L. Marques, J. L. Hodeau, O. Béthoux, M. Perroux, *Phys. Rev. Lett.* **74**, 278 (1995).
16. M. Barrio *et al.*, *Chem. Mater.* **15**, 288 (2003).
17. F. Michaud *et al.*, *Chem. Mater.* **12**, 3595 (2000).
18. L. Wang *et al.*, *Adv. Mater.* **18**, 1883 (2006).
19. A. Talyzin, U. Jansson, *J. Phys. Chem. B* **104**, 5064 (2000).
20. A. Graja, R. Swietlik, *Synth. Met.* **70**, 1417 (1995).
21. R. Swietlik, P. Byszewski, E. Kowalska, *Chem. Phys. Lett.* **254**, 73 (1996).
22. L. Wang *et al.*, *Chem. Mater.* **18**, 4190 (2006).
23. M. Ramm, P. Luger, D. Zobel, W. Duczek, J. C. A. Boeyens, *Cryst. Res. Technol.* **31**, 43 (1996).

Acknowledgments: We thank H.-k. Mao for valuable comments. We also thank Y. Xiao, G. Shen, S. Yu, V. Prakapenka, A. Kubo, Y. Zhao, W. Cui, R. Liu, and X. Huang for their help. This work was supported as part of EFree, an Energy Frontier Research Center funded by the U.S. Department of Energy (DOE), Office of Science under DE-SC0001057. The use of HPCAT, Advanced Photon Source (APS) is supported by the Carnegie Institute of Washington, Carnegie DOE Alliance Center, University of Nevada at Las Vegas, and Lawrence Livermore National Laboratory through funding from the DOE National Nuclear Security Administration, DOE Basic Energy Sciences, and National Science Foundation (NSF). The use of beamline U2A is supported by NSF (DMR-0805056; EAR 06-49658, Consortium for Materials Properties Research in Earth Sciences (COMPRES)). For the computational research, we used resources from the Oak Ridge Leadership Computing Facility at Oak Ridge National Laboratory, which is supported by the Office of Science of the DOE under contract DE-AC05-00OR22725, and from Holland Computing Center at the University of Nebraska. The synthesis and characterizations of the samples were conducted by the Jilin University group, supported by the National Natural Science Foundation of China (NSFC, 11004072) and Program for New Century Excellent Talents in University (NCET, 2010).

Supplementary Materials

www.sciencemag.org/cgi/content/full/337/6096/825/DC1
Materials and Methods
Supplementary Text
Figs. S1 to S11
References (*24*–*28*)

14 February 2012; accepted 1 June 2012
10.1126/science.1220522

Camouflage and Display for Soft Machines

Stephen A. Morin,[1] Robert F. Shepherd,[1] Sen Wai Kwok,[1] Adam A. Stokes,[1] Alex Nemiroski,[1] George M. Whitesides[1,2]*

Synthetic systems cannot easily mimic the color-changing abilities of animals such as cephalopods. Soft machines—machines fabricated from soft polymers and flexible reinforcing sheets—are rapidly increasing in functionality. This manuscript describes simple microfluidic networks that can change the color, contrast, pattern, apparent shape, luminescence, and surface temperature of soft machines for camouflage and display. The color of these microfluidic networks can be changed simultaneously in the visible and infrared—a capability that organisms do not have. These strategies begin to imitate the functions, although not the anatomies, of color-changing animals.

Cephalopods (such as squid and cuttlefish) have amazing control over their appearance (color, contrast, pattern, and shape) (*1*, *2*). These animals use dynamic body patterns for disguise, for protection, and for warning. Other animals (such as chameleons and many insects) can also actively change their coloration for camouflage or display (*3*, *4*). Still others (such as jellyfish and fireflies) use bioluminescence to communicate (*5*). The color-changing capabilities of these animals have not been replicated by using soft synthetic systems, but such systems could enhance the function of certain machines (such as robots or prosthetics).

This paper describes our initial approaches to change the color, contrast, pattern, apparent shape, luminescence, and infrared (IR) emission (that is, surface temperature) of soft machines fabricated from elastomers and flexible reinforcing sheets (*6*–*8*) by changing the color and pattern of microfluidic networks. These systems are first steps toward imitating the functions, although not the anatomies, of cephalopods (*9*, *10*) and other color-changing animals (*4*). These animals typically change color using specialized cells, such as chromatophores or iridophores (*4*, *9*, *10*), not simple microchannels. The near-perfect matching of environments used by color-changing organisms with highly developed nervous systems is not required for camouflage to be effective.

Nature offers countless examples of camouflage and display (*3*, *11*, *12*). Although specific demonstrations of camouflage vary among species, the strategies used have common themes: background matching, disruptive coloration, and disguise (*3*, *11*, *12*). In background matching, animals use colors and patterns similar to their habitats (*3*, *11*–*13*), such as counter/obliterative shading (for example, rabbits with white underbellies and brown backs) (*11*, *12*). Disruptive coloration breaks up the silhouette of an animal using contrasting patterns that do not follow its shape (*3*). Disguise is a strategy in which an organism adopts the shape and color of objects or animals in the environment (such as stick insects and phasmida) (*3*). Display strategies are used for communication, mating, and hunting and can be just as critical for survival as camouflage (*3*). Bioluminescence is commonly used for display in low- or no-light conditions (*5*, *14*); when lighting is strong, animals sometimes advertise themselves by combining vibrant contrasting colors with distinct shapes (*15*–*17*). For example, jellyfish use bioluminescence to warn would-be predators (*5*), and peacocks use bright plumage to attract mates (*18*).

Although most strategies of camouflage and display (*3*, *12*) emphasize the visible spectrum that most animals (especially mammals) can see (*19*–*21*), there are animals that can see (or otherwise sense) ultraviolet (UV) or IR light and use these spectral regions for signaling or hunting. For example, most birds, many arthropods, and some fish have UV vision (*22*), and many snakes, such as pit vipers, can sense IR light using specialized organs (*23*). Semiconductor technology has expanded our ability to see into the IR (*24*), and we explored techniques for camouflage or display in the IR.

Our system combines microfluidics, pattern, and color to provide both camouflage/display and movement of the soft machines. Camouflage or display results from pumping colored or temperature-controlled fluids through a network of microfluidic channels; mechanical actuation results from pneumatic pressurization and inflation of an independent network of microchannels (pneu-nets) embedded in highly extensible elastomers (*6*, *7*). The microfluidic networks used for camouflage/display are contained in thin silicone sheets [Ecoflex (Smooth-On, Easton, PA), 1 to 2 mm thick] referred to as color layers (Fig. 1 and fig. S1). Although there are technologies, such as electrowetting (*25*) and electrofluidics (*26*), that use microfluidics to tune color, they rely on electric fields to move fluid and are not immediately compatible with our compressed-air power source.

The color layers are easily fabricated (*27*), can cover large areas, and can transport a variety of fluids (both liquids and gases) using similar controls (*28*). The liquids can be colored with dyes or pigments and heated/cooled to change the color of the microfluidic networks in the visible and IR

[1]Department of Chemistry and Chemical Biology, Harvard University, 12 Oxford Street, Cambridge, MA 02138, USA. [2]Wyss Institute for Biologically Inspired Engineering, Harvard University, 60 Oxford Street, Cambridge, MA 02138, USA.

*To whom correspondence should be addressed. E-mail: gwhitesides@gmwgroup.harvard.edu